Growth orientation and superconducting properties of YBa$_2$Cu$_3$O$_{7-\delta}$ films prepared by the low-fluorine sol–gel process*

Lei Li(雷黎)[†], Zhao Gaoyang(赵高扬), Xu Hui(徐慧), and Zhao Juanjuan(赵娟娟)

(School of Materials Science and Engineering, Xi'an University of Technology, Xi'an 710048, China)

Abstract: YBa$_2$Cu$_3$O$_{7-\delta}$(YBCO) films were deposited on (100)-oriented LaAlO$_3$ (LAO) single crystal substrates by the dip-coating process using low-fluorine solution. Their microstructures were characterized with the aid of X-ray diffractometry, scanning electron microscopy and high-resolution transmission electron microscopy. Their superconducting properties were measured by the standard four-probe method. The experiment results show that the film obtained under high enough humidity conditions exhibits better c-axis texture and superconducting properties than the film under a relatively low humidity conditions. Based on the classical nucleation and chemical reaction thermodynamics theory, the underlying crystalline and growth mechanisms of YBCO films under certain humidity conditions are explained in combination with our experimental results. It is suggested that the unreacted intermediate phases such as BaF$_2$ and CuO aggregated in the YBCO grain boundary will cause lattice distortion in the YBCO matrix and further induce the formation of a-axis oriented YBCO grains as crystallization proceeds. Therefore, it is believed that the relative content of water vapor within the heat-treatment atmosphere plays quite an important role in the preparation of c-axis oriented YBCO film with good superconducting properties.

Key words: YBCO films; low-fluorine process; growth orientation; sol–gel
DOI: 10.1088/1674-4926/31/8/083004   **PACC:** 7360K; 6855; 8270G

1. Introduction

Since the advent of high-temperature superconductors, much research on their development has been done over the past two decades. At present, it is universally thought that yttrium-system superconductors are the most promising high temperature superconducting materials for applications in electrical and magnetic fields. Therefore, many different methods used to fabricate YBa$_2$Cu$_3$O$_{7-\delta}$(YBCO) films or coated conductors (CC) have been developed, of which non-vacuum techniques such as metal organic decomposition (MOD)[1−3] and the sol–gel method[4, 5] have attracted great attention from many research communities due to their simple apparatus and low processing cost. Recently, the metal organic decomposition process using trifluoroacetate (TFA-MOD) was considered to be quite an effective method to prepare YBCO films[6−9] and second-generation CC[10−12]. However, using *ex-situ* chemical solution deposition methods, including MOD and sol–gel, to prepare YBCO films has several disadvantages such as chemical composition instability caused by volatilization of copper metal–organic compounds in the precursor film[13] and the non-uniformity of nucleation and growth resulting from impurity phases and heat-treatment conditions, in particular with humidity. It has been reported that the J_c value of YBCO films by the TFA-MOD method was drastically decreased due to the poor crystal alignment of the YBCO phase and a-axis oriented YBCO grains[6]. Consequently, it is quite necessary to discuss the effect of these factors on the properties of YBCO films.

In this study, two YBCO samples (one under relatively low humidity and the other with high enough humidity under which BaF$_2$ can be completely converted to YBCO) were deposited on LaAlO$_3$ (LAO) substrate by the low-fluorine sol–gel process. XRD, SEM and HRTEM have been used to confirm the nucleation and growth mechanism of the YBCO films. We study the contribution of water vapor within the furnace atmosphere to a-/c-axis texture formation and superconducting properties of low-fluorine based YBCO films, and explain the underlying growth mechanism of YBCO films.
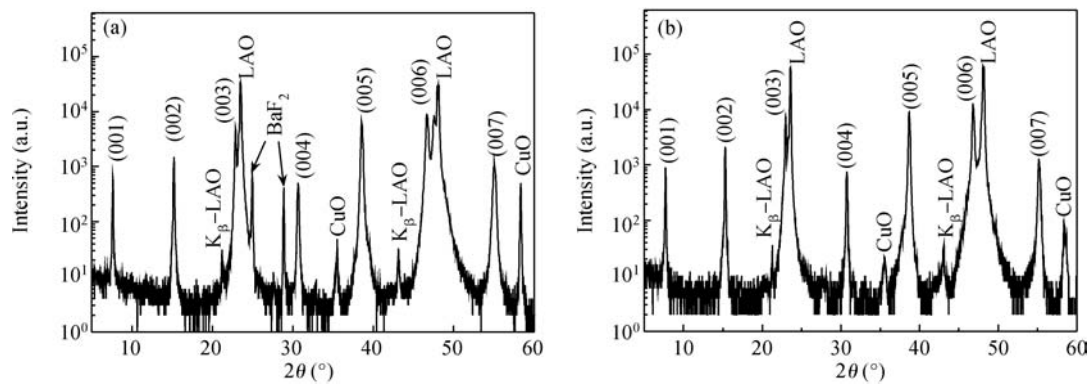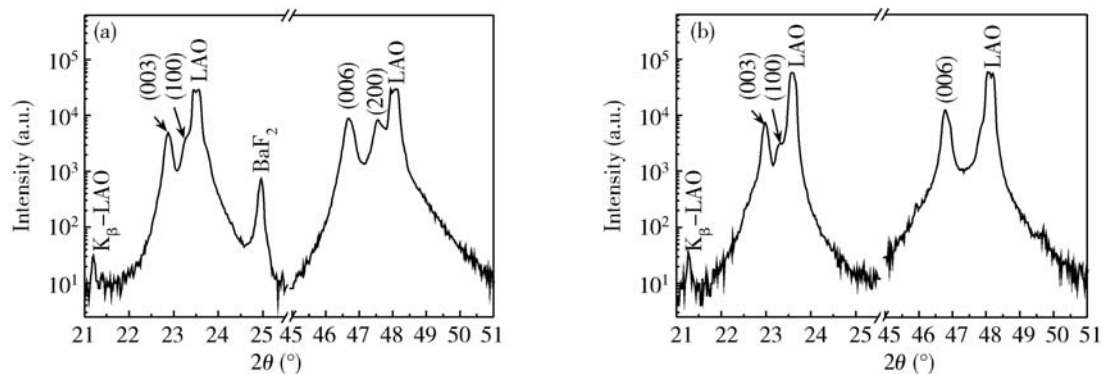
2. Experimental

Yttrium acetate (Y(OAc)$_3$) and cuprum acetate (Cu(OAc)$_2$) were dissolved in methanol (MeOH) using diethylenertiamine (DETA) and α-methacrylic acid as a chelating agent respectively to prepare stable solution 1 and solution 3, while barium acetate (Ba(OAc)$_2$) was first dissolved in de-ionized water with a stoichiometric quantity of trifluoroacetic acid at room temperature, and then water and acetic acid were dried in an oven with the temperature controlled at 75 ℃. A transparent glassy residue, namely Ba-TFA, was obtained. Solution 2 was prepared by dissolving the glassy residue in MeOH. The three solutions above were respectively stirred on magnetic-force stirrers to make them clear and transparent. Ultimately, stable YBCO precursor solution (low-fluorine solution) was obtained by mixing these three solutions together and stirring for several hours. The molar ratio of metallic ions was controlled at a stoichiometry of Y^{3+}: Ba^{2+}: Cu^{2+}= 1 : 2 : 3.8. Here, 26.7% Cu excess is adopted to compensate for Cu loss during the pyrolysis process[13]. The solution concentration was controlled at

† Corresponding author. Email:leili813@gmail.com

Fig. 1. XRD θ–2θ scan patterns of (a) film A and (b) film B.

Fig. 2. Enlarged XRD θ–2θ scan patterns of (a) film A and (b) film B.

1.5 mol/L (calculated in terms of the total molar quantity of metallic ions in solution) by adjusting the amount of methanol used.

YBCO precursor films were coated on (100)-oriented LAO single crystal substrate with dimensions $10 \times 10 \times 1$ mm^3 using the dip-coating process. The thickness of the films can be controlled by adjusting the dip-coating speed. Two YBCO films were obtained under two given heat treatment conditions, where the heat treatment temperature and the oxygen partial pressure were kept at 800 ℃ and 1000 ppm respectively with different humidities of dew point (D.P.) 35 ℃ for film A and D.P. 50 ℃ for film B. The detailed heat-treatment process was mentioned in our previous paper[14].

A Shimadzu Ltd 7000S X-ray diffractometer with CuKα radiation XRD θ–2θ scan was used to carry out the crystal structure and orientation analysis. Micro-morphology of as-prepared YBCO films was observed by JEOL JSM-6700F scanning electron microscopy (SEM). The interface structure of YBCO films was studied by JEOL 3010F high-resolution transmission electron microscopy (HRTEM). The superconducting properties of the YBCO films were measured by the standard four-probe method.

3. Results and discussion

3.1. XRD, SEM and TEM characterization

In order to clearly distinguish the diffraction peaks of impurities, logarithmic coordinates were used in the XRD patterns. Figure 1 shows X-ray diffraction θ–2θ scan patterns of

YBCO films on LAO substrate derived from low-fluorine solution. Figures 1(a), 1(b) are the XRD patterns of film A (800 ℃, 1000 ppm, D.P. 35 ℃) and film B (800 ℃, 1000 ppm, D.P. 50 ℃) respectively. It can be seen that the diffraction peaks of the YBCO (00l) planes in the two patterns are quite strong and sharp, which indicates that YBCO films mainly grow along the c-axis orientation on LAO substrate. However, peaks of the (100), (200) planes corresponding to a-axis oriented YBCO grains can also be seen in Fig. 1 (a), which implies that there is a certain quantity of a-axis grains in film A. Figure 2 shows the enlarged diffraction peaks of the (003), (100), (006) and (200) planes in Fig. 1. As shown in Fig. 2, the 2θ value corresponding to the diffraction peaks of film A is slightly less than that of film B, which may result from the deficiency of oxygen content in film A. Lack of oxygen content can often have a bad effect on the superconducting properties of YBCO films (for detailed discussions please see section 3.2). In order to make a quantitative analysis, we calculated the volume fraction $\alpha_{(00l)}$ of c-axis oriented grains in YBCO films according to a calculation formula (please see Ref. [15]) of preferred orientation degree. The $\alpha_{(00l)}$ values calculated for films A and B are 56.38% and 92.36% respectively. In addition, two diffraction peaks at 2θ of 24.95° and 28.93° corresponding to the BaF$_2$ phase and another two peaks at 35.52° and 58.32° corresponding to the CuO phase were also observed in Fig. 1(a), which suggests that there are some unreacted intermediate phases remaining in film A, while two diffraction peaks of the CuO phase were only detected in film B, except for the peaks of YBCO and LAO. We believe that the CuO phase remaining in film B may be asso-
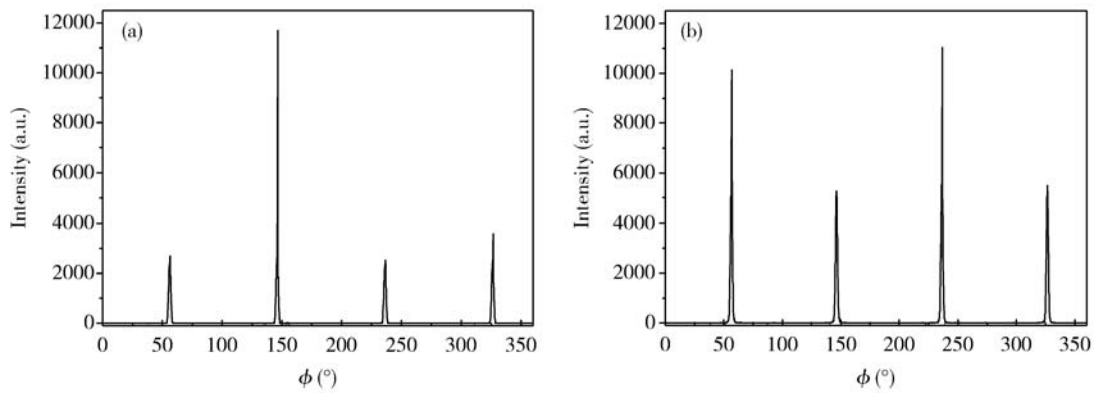
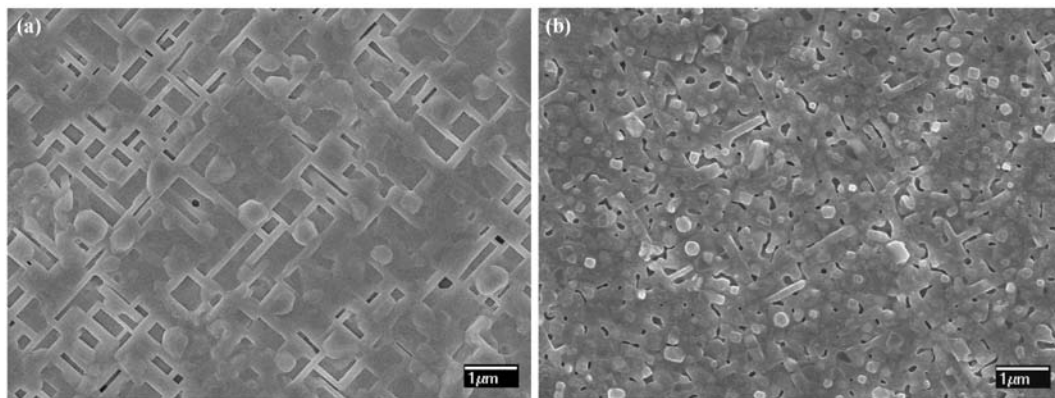Fig. 3. XRD ϕ-scan patterns of (a) film A and (b) film B.

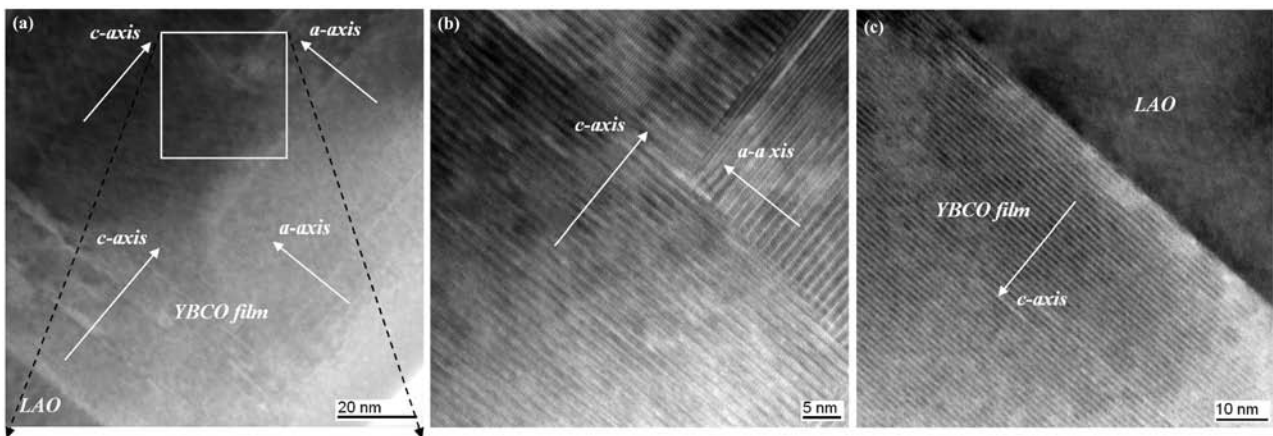Fig. 4. Surface morphology of (a) film A and (b) film B.

Fig. 5. Cross-section HRTEM images of the YBCO films. (a) Interface between c-axis and a-axis oriented YBCO grains in film A. (b) Enlarged image of the rectangular zone in (a). (c) c-axis oriented growth in film B.

ciated with the excess of Cu in the YBCO precursor solution. The in-plane texture of YBCO films were measured by XRD ϕ-scan. Figures 3(a) and 3(b) show the (103) ϕ-scan patterns of films A and B respectively. The full-width at half-maximum (FWHM) of film B is 1.13° less than that (FWHM 2.56°) of film A, which indicates that film B has a better in-plane texture than film A.

SEM micrographs of YBCO films are shown in Fig. 4. Large quantities of needle-like a-axis grains[16, 17] on the surface of film A can be seen in Fig. 4(a), while film B exhibits the growth characteristic of island-like c-axis grains including a few a-axis grains, as shown in Fig. 4(b). This result is very consistent with the above XRD analysis.

HRTEM was performed to further characterize the internal structures of YBCO films. Figure 5 shows cross-section HRTEM images of the YBCO films. Therein, Figure 5(a) shows a coexisting structure feature of c- and a-axis oriented YBCO grains, and the a-axis grains began to form approximately 30 nm away from the LAO substrate. A close-up view of the rectangular zone in Fig. 5(a) is presented in Fig. 5(b),
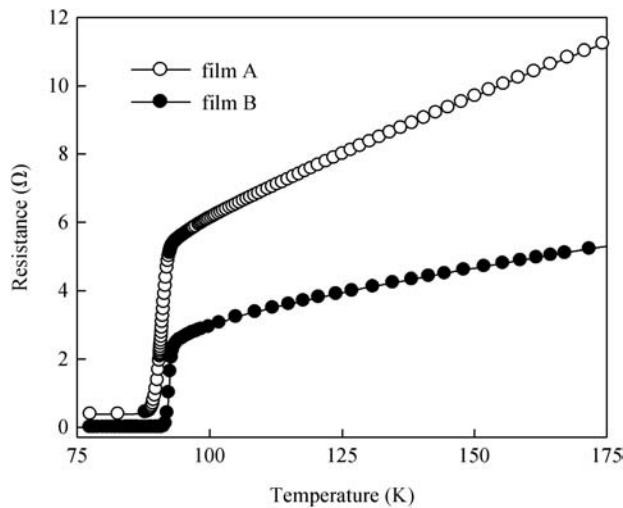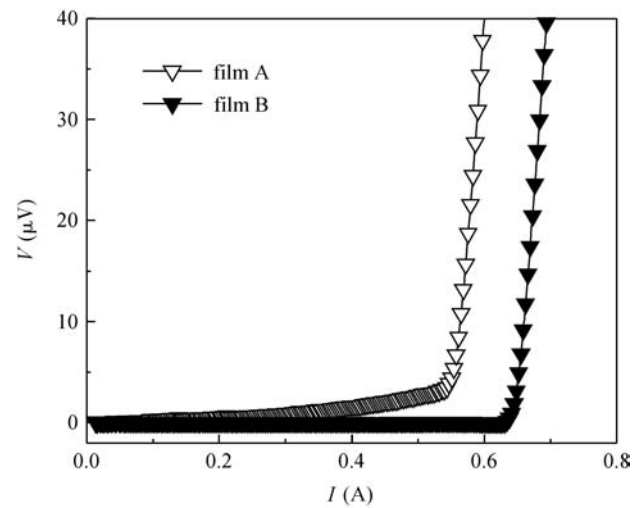
Fig. 6. $R-T$ curves of the YBCO films.

Fig. 7. $V-I$ curves of the YBCO films.

from which the clear interface between a- and c-axis grains angled at 90 degrees to each other can be seen. An HRTEM image of film B grown on LAO substrate is shown in Fig. 5(c), in which YBCO film grown along the c-axis direction perpendicular to the YBCO/LAO interface maintains a good coherence relation with the LAO substrate and no amorphous transition area is observed. It is believed that the different growth characteristics of the two YBCO samples can be attributed to the different humidity conditions.
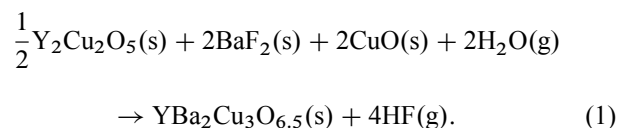
3.2. Superconducting properties test

The dependence of resistance on temperature ($R-T$ curve) of the YBCO films is shown in Fig. 6. It can be seen from Fig. 6 that film A shows a wide superconducting transition width (ΔT) and a resistance value of 0.5 Ω when the temperature is decreased to 77 K, while film B exhibits a sharp superconducting transition. The critical transition temperature T_c and ΔT of film B are about 92 K and 0.84 K (less than 1 K) respectively. As we all know, the superconducting-normal transition in $YBa_2Cu_3O_{7-\delta}$ can only occur when the oxygen content is more than 6.5 (i.e. $\delta < 0.5$). Large δ usually leads to low T_c and wide ΔT. According to the above XRD results, the wide ΔT and resistance state of film A at 77 K can be attributed to the low oxygen content in YBCO. It is believed that the oxygen atoms in H_2O will enter the YBCO lattice through the reaction of YBCO phase formation (please see section 3.3) and a higher humidity will provide more oxygen for YBCO.

Figure 7 shows the transport voltage–current curve ($V-I$ curve) of the YBCO films. Films A and B were patterned to be micro-bridges with a width of 200 μm and a thickness of 0.29 μm and 0.26 μm respectively. The critical current of film B is 0.64 A with a criterion of 1 μV/cm, which corresponds to a critical current density J_c of 1.23 MA/cm^2 (77 K, 0 T). The high J_c of film B is attributed to excellent c-axis growth orientation and dense microstructure with good intergranular connectivity. In addition, it is noticed that the $V-I$ curve of film A shows a turning point like that in the curve of film B, which indicates that non-superconducting phases and a superconducting YBCO phase coexist in film A.

3.3. Explanation of underlying growth mechanism

It is known that heat treatment process parameters, such as temperature and atmosphere, have a great influence on the structure and properties of YBCO films. As shown above, film B with good c-axis texture exhibits better superconductivity than film A with a large quantity of a-axis grains and impurities only due to the slight variation of the heat treatment process conditions, which indicates that water vapor may play a key role in the formation of YBCO grain orientation. Therefore, we attempt to discuss and explain the underlying crystalline and growth mechanisms of YBCO films.

In the preparation of YBCO films using fluorine-contained solution, YBCO gel films are pyrolyzed to form a precursor film comprised of yttrium, barium and cuprum oxides and fluorides during the pre-treatment process. It was reported that the pyrolyzed precursor film is composed of $Y_2Cu_2O_5$, CuO and BaF_2 phases, and these oxides and fluorides can be reacted with H_2O to produce the YBCO phase during the high-temperature heat-treatment process. The formation of the YBCO phase can be interpreted by the following reaction (1)[6, 18]. For epitaxial YBCO films using *ex-situ* chemical solution deposition, it is well known that crystallization begins in the interface between the amorphous YBCO precursor and single crystal substrate, and as crystallization proceeds the boundary between the amorphous precursor and crystallized YBCO phase moves to the amorphous region until the precursor film is completely converted into the YBCO phase.

$$\frac{1}{2}Y_2Cu_2O_5(s) + 2BaF_2(s) + 2CuO(s) + 2H_2O(g)$$

$$\rightarrow YBa_2Cu_3O_{6.5}(s) + 4HF(g). \qquad (1)$$

However, there are several unreacted reactants remaining in the final YBCO films as impurities when the water vapor content within the annealing atmosphere is inadequate. For reaction (1), the equilibrium constant K can be expressed by

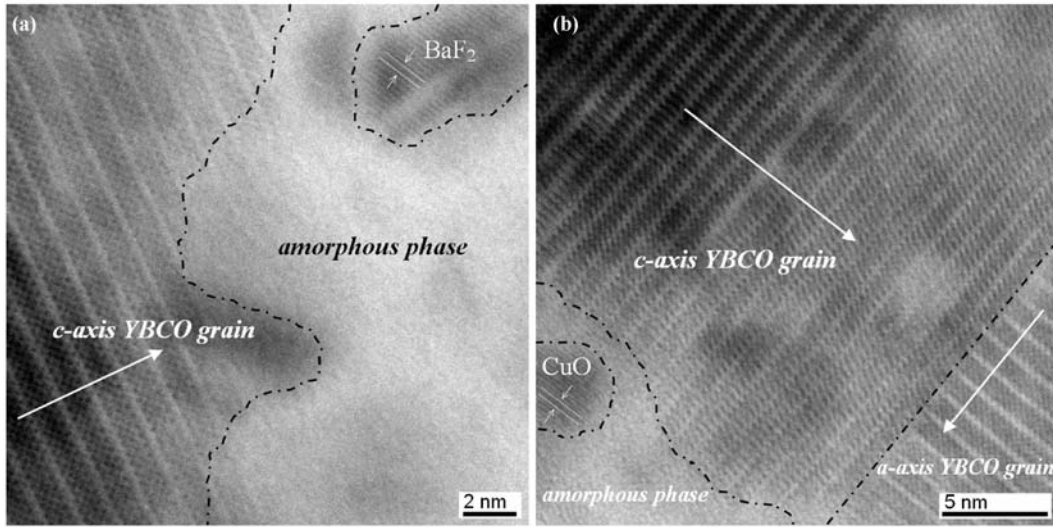$$K = \frac{a_{YBCO}P_{HF}^4}{a_{Y_2Cu_2O_5}^{1/2}a_{BaF_2}^2a_{CuO}^2P_{H_2O}^2}. \qquad (2)$$

Fig. 8. Cross-section HRTEM images of film A. (a) Interface of c-axis YBCO grains and amorphous phase. (b) Interface of c-axis and a-axis YBCO grains.

Assuming that if the activity of the solid phase is constant, Equation (2) can be simplified as

$$K = \alpha \frac{P_{HF}^4}{P_{H_2O}^2}, \qquad (3)$$

where α is a constant. According to the van 't Hoff isothermal equation, the reaction molar Gibbs function at temperature T can be calculated by

$$\Delta_r G_m(T) = RT \ln \frac{Q_p}{K_p^{\Theta}(T)}, \qquad (4)$$

where $Q_p = P_{HF}^4/P_{H_2O}^2$, $K_p^{\Theta}(T)$ is the standard equilibrium constant at temperature T. The reaction (1) can be always forced to the right until the $Y_2Cu_2O_5$, CuO and BaF_2 phases are completely converted into YBCO phase when the water vapor partial pressure reaches a certain value (i.e. $\Delta_r G_m(T) < 0$). In this paper, as shown in the above XRD analysis, the relatively low humidity induced the unreacted BaF_2 impurity phase in film A. Also, the excessive BaF_2 phase in film A can be clearly observed by HRTEM (as shown in Fig. 8(a)). For the *ex-situ* deposition of YBCO films derived from chemical solution, the second phases are usually surrounded by amorphous phase; this is the reason why these second phases as impurities remain inside the amorphous phase region when the reaction is not completely carried out. Nanocrystalline CuO is easily formed during the YBCO nucleation process and exists steadily in the YBCO films (as shown in Fig. 8(b)).

It is well known that YBCO film nucleation and growth on LAO substrate is the heteroepitaxial growth mode, which is an induced nucleation by the substrate. Whether the epitaxial growth can proceed or not, according to the classic nucleation theory, is mostly determined by the value of total free-energy change ΔG_{het} when epitaxial film is adhered to the substrate to form a crystal nucleus. The total free-energy change can be expressed as

$$\Delta G_{het} = V \cdot \Delta G_V + A_1 \gamma_{n-v} + A_2 (\gamma_{s-n} - \gamma_{s-v}), \qquad (5)$$

where ΔG_V is the volume free-energy change, γ_{n-v} is the surface tension of the nucleus, γ_{s-n} is the interface energy of the crystal nucleus and substrate, and γ_{s-v} is the surface energy of the substrate. V, A_1 and A_2 are the volume, cap surface area and projected area of the crystal nucleus respectively. It is known that the lattice constants of LAO and YBCO are $a_{LAO} = b_{LAO} = c_{LAO} = 3.792$ Å, $a_{YBCO} = 3.817$ Å, $b_{YBCO} = 3.884$ Å and $c_{YBCO} = 11.68$ Å respectively. According to Eq. (5), we can calculate the total free-energy change ΔG_a^* and ΔG_c^* when a-axis and c-axis grains nucleate. The calculation results are $\Delta G_a^* = V\Delta G_V + (3ac + 2a^2)\Upsilon_{n-v} + ac(\Upsilon_{s-n} - \Upsilon_{s-v})$ and $\Delta G_c^* = V\Delta G_V + (4ac + a^2)\Upsilon_{n-v} + a^2(\Upsilon_{s-n} - \Upsilon_{s-v})$. The shape of the YBCO nucleus is a quadrangular prism whether the c-axis or a-axis grains nucleate, therefore $\Delta G_c^* - \Delta G_a^* = (ac - a^2)(\Upsilon_{n-v} + \Upsilon_{s-v} - \Upsilon_{s-n})$. Since $(ac - a^2) > 0$ ($a < c$) and $\Upsilon_{n-v} + \Upsilon_{s-v} - \Upsilon_{s-n} = \sigma_{ad} = u_{n-s}/a^2 > 0$ (here, σ_{ad} is the adhesional energy between the YBCO nucleus and the LAO substrate; u_{n-s} is the bond energy between the atoms of the nucleus and the substrate), $\Delta G_c^* - \Delta G_a^* > 0$ (i.e. $\Delta G_a^* < \Delta G_c^*$), which indicates that a-axis oriented YBCO grains nucleate more easily on LAO substrate than c-axis YBCO grains. According to the chemical thermodynamics theory, however, in the reaction (1), ΔG_V is the function of ΔT, P_{H_2O} and P_{HF}; this functional relationship can be expressed by

$$\Delta G_V = \Delta G_V^{\Theta} + RT \ln \left[(P_{HF})^4 \big/ (P_{HF})^4 (P_{H_2O})^2 \right]$$
$$= R \cdot \Delta T \ln \left[(P_{HF})^4 \big/ (P_{HF})^4 (P_{H_2O})^2 \right], \qquad (6)$$

where ΔG_V^{Θ} is the standard free-energy change, R is the gas constant, T is the actual temperature during nucleation and growth, ΔT is the D-value between the actual temperature and the equilibrium state temperature, P_{HF} is the HF gas partial pressure and P_{H_2O} is the H_2O vapor partial pressure. In the actual process, $P_{H_2O} \gg P_{HF}$ (i.e. $(P_{HF})^4/(P_{H_2O})^2 < 1$), thus Equation (6) suggests that elevating T (i.e. increasing ΔT) or increasing P_{H_2O} can make the absolute value of ΔG_V increase, thus resulting in the increase of YBCO heterogeneous nucle-
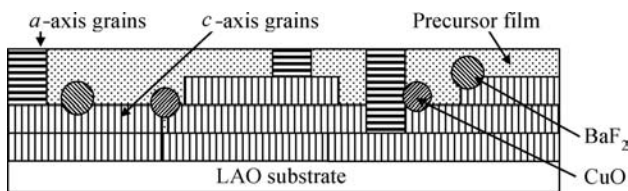
Fig. 9. Schematic diagram of nucleation and growth for YBCO film.

ation energy ΔG_{het}. According to the above discussion, $\Delta G_a^* < \Delta G_c^*$, thus the nucleation of c-axis oriented YBCO grains becomes possible due to the relatively large ΔG_{het}. As a general rule, YBCO begins to nucleate around a temperature of 700 ℃ at low oxygen partial pressure. In addition, with the increase of temperature, the lattice constants of YBCO and LAO will increase and c_{YBCO} increases more rapidly than a_{YBCO}, b_{YBCO} and a_{LAO} when the temperature is greater than 700 ℃[19, 20]. Therefore, in our case, at a high temperature of 800 ℃, the nucleation of a-axis grains will induce a larger strain energy than c-axis grains on the LAO substrate due to the larger ratio of $c_{\text{YBCO}}'/c_{\text{YBCO}}$ than $a_{\text{YBCO}}'/a_{\text{YBCO}}$ (here, a_{YBCO}, c_{YBCO} and a_{YBCO}', c_{YBCO}' are the lattice constants of YBCO when the temperature was lower than 800 °C and stayed at 800 °C respectively; $c_{\text{YBCO}}' > c_{\text{YBCO}}$ and $a_{\text{YBCO}}' > a_{\text{YBCO}}$, which indicates that the YBCO phase should preferentially nucleate and grow along the c-axis direction on the LAO substrate. This can be confirmed by the HRTEM results shown in Fig. 5.

However, intermediate phases such as Y_2O_3, BaF_2 and CuO usually aggregate at the YBCO grain boundary which can enlarge the YBCO intergranular angle and cause lattice distortion as crystallization proceeds. The extra lattice distortion energy can make the total free-energy of the system increase. In this case, if c-axis grains continue to nucleate and grow, there will be more internal distortion energy stored in the YBCO matrix. This is unfavorable and even impossible according to the lowest energy principle. Instead, the nucleation of a-axis grains may release some distortion energy due to their low nucleation energy ΔG_a^*. Consequently, a-axis oriented YBCO grains usually appear on the top surface of YBCO films even though almost all of the internal grains grow along the c-axis direction (as shown in Fig. 4(b)). If there are some unreacted intermediate phases left in the YBCO film, a larger strain energy can be induced which can result in more a-axis YBCO grains (as shown in Fig. 4(a)). A schematic diagram of nucleation and growth for YBCO film is shown in Fig. 9.

From the above analysis and discussion, we conclude that relatively low humidity can lead to impurity phases and the formation of a-axis oriented YBCO grains, while large enough humidity can completely convert the $Y_2Cu_2O_5$, CuO and BaF_2 phases into the YBCO phase and facilitate the formation of c-axis oriented YBCO grains, thus resulting in excellent superconducting performance. Consequently, it is crucial to control the water content within the atmosphere for preparation of YBCO film with high c-axis orientation.

4. Conclusion

YBCO films were deposited on LAO substrate by the low-fluorine sol–gel process. Under certain process conditions,

maintaining the post-treatment temperature at 800 °C and the oxygen partial pressure at 1000 ppm respectively with different humidities of D.P. 35 °C for film A and D.P. 50 °C for film B, the crystalline and growth mechanisms of YBCO films are analyzed and discussed by XRD, SEM and HRTEM in combination with classical nucleation theory and the chemical thermodynamics principle. It is learned that relatively low humidity can lead to unreacted phases remaining in YBCO films as impurities, resulting in the formation of a-axis oriented YBCO grains, while large enough humidity can produce c-axis oriented YBCO film. Lattice distortion caused by the aggregation of impurity phases may be a reason for inducing the formation of a-axis oriented YBCO grains. HRTEM observations indicate that there are good coherence and epitaxy relations (without any amorphous transition areas) between YBCO film and LAO substrate. Superconducting property tests show that a relatively low humidity within the atmosphere leads to the low oxygen content and poor superconductivity of film A, while a large enough humidity makes film B exhibit good c-axis texture and excellent superconducting properties with a high T_c of 92 K, sharp transition ΔT of 0.84 K and J_c of 1.23 MA/cm^2 (77 K, 0 T).

References

[1] Jee Y A, Ma B, Maroni V A, et al. Texture development and superconducting properties of $YBa_2Cu_3O_x$ thin films prepared by a solution process in low oxygen partial pressure. Supercond Sci Tech, 2001, 14(5): 285

[2] Yamagiwa K, Araki T, Takahashi Y, et al. Epitaxial growth of $REBa_2Cu_3O_{7-y}$ films on various substrates by chemical solution deposition. J Cryst Growth, 2001, 229(1): 353

[3] Tokunaga Y, Fuji H, Teranishi R, et al. High critical current YBCO films using advanced TFA-MOD process. Physica C, 2004, 412–414: 910

[4] Risse G, Schlobach B, Hassler W, et al. Textured YBCO-film formation by sol–gel process and post annealing. J Eur Ceram Soc, 1999, 19(1): 125

[5] Shi D L, Xu Y L, Wang S X, et al. Deposition and interface structures of YBCO thin films via a non-fluorine sol–gel route. Physica C, 2002, 371(2): 97

[6] Smith J A, Cima M J, Sonnenberg N. High critical current density thick MOD-derived YBCO films. IEEE Trans Appl Supercon, 1999, 9(2): 1531

[7] Niwa T, Araki T, Muroga T, et al. Calcining conditions for $YBa_2Cu_3O_{7-x}$ films by metalorganic deposition using trifluoroacetates. IEEE Trans Appl Supercon, 2003, 13(2): 2747

[8] Araki T, Yamagiwa K, Hirabayashi I, et al. Large-area uniform ultrahigh-J_c $YBa_2Cu_3O_{7-x}$ film fabricated by the metalorganic deposition method using trifluoroacetates. Supercond Sci Tech, 2001, 14(7): L21

[9] Sohma M, Yamaguchi I, Tsukada K, et al. Cerium oxide (CeO_2) buffer layers for preparation of high-J_c YBCO films on large-area sapphire substrates (30 cm × 10 cm) by coating pyrolysis. Physica C, 2004, 412-414: 1326

[10] Tokunaga Y, Honjo T, Izumi T, et al. Advanced TFA-MOD process of high critical current YBCO films for coated conductors. Cryogenics, 2004, 44(11): 817

[11] Fuji H, Honjo T, Teranishi R, et al. Processing for long YBCO coated conductors by advanced TFA-MOD process. Physica C, 2004, 412–414: 916

[12] Nakanishi T, Yoshizumi M, Matsuda J, et al. Fabrication of long

Y123 coated conductor tape by advanced TFA-MOD process. Physica C, 2007, 463: 515

[13] Dawley J T, Clem P G, Boyle T J, et al. Rapid processing method for solution deposited $YBa_2Cu_3O_{7-\delta}$ thin films. Physica C, 2004, 402(1/2): 143

[14] Zhao G Y, Chen Y Q, Lei L, et al. Fabrication of $YBa_2Cu_3O_{7-x}$ superconducting films using low-fluorine-content solution. IEEE Trans Appl Supercon, 2007, 17(1): 40

[15] Zhao G Y, Lei L, Liu X M, et al. Effect of copper content in precursor solution on the superconducting properties of YBCO films derived from low-fluorine solution. Physica C, 2008, 468(23): 2317

[16] Leibovitch G, Beck R, Deutscher G. High quality a-axis out-growth on c-axis $Y_{1-x}Ca_xBa_2Cu_3O_{7-\delta}$. Supercond Sci Technol, 2004, 17: 1065

[17] Mizuno Y, Ishimaru Y, Wen J, et al. Fabrication of $NdBa_2Cu_3O_{7-\delta}$ (110)-(001) grain boundary josephson junction by focused ion beam method. Jpn J Appl Phys, 1997, 36: L764

[18] Teranishi R, Fuji H, Honjo T, et al. Growth mechanism of Y123 film by MOD-TFA process. Physica C, 2002, 378: 1033

[19] Poole C, Farach H, Creswick R. Handbook of superconductivity. Academic Press New York, 2000

[20] Xu Y. High J_c epitaxial $YBa_2Cu_3O_{7-\delta}$ films through a non-fluorine approach for coated conductor application. Cincinnati: University of Cincinnati, 2003